

Electronic Raman scattering in $\text{Ti}_2\text{Ba}_2\text{CuO}_{6+\delta}$: symmetry of the order parameter, oxygen doping effects, and normal state scattering

L.V. Gasparov

2. Physikalisches Institut, RWTH-Aachen, 52056 Aachen, Germany and Institute for Solid State Physics, 142432, Chernogolovka, Moscow district, Russia

P. Lemmens

2. Physikalisches Institut, RWTH-Aachen, 52056 Aachen, Germany

N.N. Kolesnikov

Institute for Solid State Physics 142432, Chernogolovka, Moscow district, Russia

G. Güntherodt

2. Physikalisches Institut, RWTH-Aachen, 52056 Aachen, Germany

(August 11, 2018)

74.25.Gz, 74.72.Fq, 78.30.-j

Single crystals of the optimally doped, moderately and strongly overdoped high temperature superconductor $\text{Ti}_2\text{Ba}_2\text{CuO}_{6+\delta}$ (Ti-2201) with $T_c=80$, 56 and 30 K, respectively, have been investigated by polarized Raman scattering. By taking the peak position of the B_{1g} component of electronic Raman scattering as $2\Delta_0$ we found that the reduced gap value ($2\Delta_0/k_B T_c$) strongly decreases with increasing doping. The behavior of the low frequency scattering for the B_{1g} and B_{2g} scattering components is similar for optimally doped and overdoped crystals and can be described by a ω^3 - and ω -law, respectively, which is consistent with a d-wave symmetry of the order parameter. In contrast to the optimally doped Ti-2201 in both, moderately and strongly overdoped Ti-2201, the relative (compared to the B_{1g}) intensity of the A_{1g} scattering component is suppressed. We suggest that the van Hove singularity is responsible for the observed changes of Raman intensity and reduced gap value with doping. Electronic Raman scattering in the normal state is discussed in the context of the scattering from impurities and compared to the existing infrared data. The scattering rate evaluated from the Raman measurements is smaller for the overdoped samples, compared to the moderately overdoped samples.

74.25.Gz, 74.72.Fq, 78.30.-j

INTRODUCTION

The symmetry of the order parameter is one of the most important questions for the high temperature superconductors (HTSC). This issue is especially interesting as a function of different doping levels. Electronic Raman scattering (ELRS) plays a special role in addressing this problem¹⁻⁷. The symmetry properties of the order parameter can be determined by investigating the anisotropy of the scattering cross section for the different symmetry components. Different scattering components originate from different areas of the Fermi surface (FS). The ratio of one scattering component compared with another one reflects the changes of the Fermi surface (FS) topology with doping⁸. There are several theoretical attempts³⁻⁷ to describe the electronic Raman scattering in HTSC at $T < T_c$, but still there is no consensus concerning the exact mechanism of the scattering.

In the optimally doped HTSC the electronic Raman scattering from single crystals in the superconducting state reveals several common features^{3-7,9-16}. The superconducting transition manifests itself in a redistribution of the ELRS continuum into a broad peak (pair-breaking peak), the intensity and frequency position Ω of which differs for the different symmetry components. For the optimally doped samples, one has $\Omega(B_{1g}) > \Omega(B_{2g}) > \Omega(A_{1g})$ ^{3-7,9-16}. The scattering on the low frequency side of the pair-breaking peak does not reveal additional peaks or a cut-off, which would be an indication of anisotropic s-wave component. In contrast, a power-law decrease of the scattering intensity toward zero frequency shift is observed. In the B_{1g} scattering component this power-law is close to a ω^3 -dependence, while in the A_{1g} and B_{2g} scattering components a linear-in- ω decrease is observed. The above mentioned features were first described by Devereaux et al.³ in the framework of a d-wave order parameter, i.e. using the gap function $\Delta(\vec{k}) = \Delta_{max} \cos 2\phi$, where ϕ is an angle between \vec{k} and Cu-O bond direction within the CuO_2 plane.

The general description of the Raman scattering cross section follows from the fluctuation-dissipation theorem. For the case of nonresonant scattering the Raman scattering cross section is given by the Raman response function $\chi_{\gamma,\gamma}(\vec{q}, \omega :)$

$$\frac{\partial^2 \sigma}{\partial \omega \partial \Omega} \propto [1 + n(\omega)] \Im \chi_{\gamma\gamma}(\vec{q}, \omega), \quad (1)$$

where $n(\omega) = 1/(\exp(\omega/T) - 1)$ is the Bose-factor, $\omega = \omega_I - \omega_S$, is Stokes Raman shift, where $\omega_I(\omega_S)$ is the frequency of the incident (scattered) photon.

The Raman response function due to the breaking of Cooper pairs in a superconductor and including Coulomb repulsion can be written as^{1,2}:

$$\chi_{\gamma\gamma}(\vec{q}, \omega) = \langle \gamma_{\vec{k}}^2 \lambda_{\vec{k}} \rangle - \frac{\langle \gamma_{\vec{k}} \lambda_{\vec{k}} \rangle^2}{\langle \lambda_{\vec{k}} \rangle}, \quad (2)$$

where $\gamma_{\vec{k}}$ is the Raman vertex, which describes the strength of the corresponding Raman transition, $\lambda_{\vec{k}}$ is the Tsuneto function¹⁷ and the brackets $\langle \dots \rangle$ denote the average of the momentum \vec{k} over the Fermi surface.

The Tsuneto function is determined as:

$$\lambda(\vec{k}, i\omega) = \frac{\Delta(\vec{k})^2}{E(\vec{k})} \tanh \left[\frac{E(\vec{k})}{2T} \right] \left[\frac{1}{2E(\vec{k}) + i\omega} + \frac{1}{2E(\vec{k}) - i\omega} \right], \quad (3)$$

with excitation energy $E^2(\vec{k}) = \xi^2(\vec{k}) + \Delta^2(\vec{k})$, conduction band $\xi(\vec{k}) = \epsilon(\vec{k}) - \mu$, chemical potential μ and superconducting energy gap $\Delta(\vec{k})$.

There is an important consequence following from Eqs. 2 and 3 that the Raman response is proportional to the square of the superconducting order parameter, therefore, as it was already mentioned in Ref. 5, Raman scattering is not sensitive to the sign of the order parameter.

In the case of nonresonant scattering one can describe the Raman vertex through the curvature of the energy bands $\epsilon(\vec{k})$:

$$\gamma_{\vec{k}} = \sum_{\alpha\beta} e_{\alpha}^I \frac{\partial^2 \epsilon(\vec{k})}{\partial k_{\alpha} \partial k_{\beta}} e_{\beta}^S, \quad (4)$$

where $\vec{e}^I(\vec{e}^S)$ is the polarization vector of the incident (scattered) photon, and α and β are summation indices which correspond to the different projections of \vec{k} .

If one assumes³ that the Raman vertex does not depend on the frequency of the incident photon one can take into account symmetry considerations to evaluate corresponding Raman scattering components. In such a case the Raman vertex can be described in terms of Brillouin zone (BZ) or Fermi surface harmonics³ $\Phi_L(\vec{k})$, which transform according to point group transformations of the crystal.

$$\gamma_{\vec{k}}(\omega_i, \omega_s) = \sum_L \gamma_L(\omega_i, \omega_s) \Phi_L(\vec{k}). \quad (5)$$

For tetragonal symmetry one gets the following form of the Raman vertices³:

$$\gamma_{B_{1g}} \propto \cos 2\phi \quad \gamma_{B_{2g}} \propto \sin 2\phi \quad \gamma_{A_{1g}} \propto 1 + \cos 4\phi. \quad (6)$$

Let us analyze the Raman response (Eq.2). For simplicity we have drawn in Fig.1 corresponding polar plots of the functions contained in each of the two terms of the Raman response. The first term is the "bare" Raman response which reflects the attractive interaction in the Cooper pair whereas the second term ("screening") is due to the Coulomb repulsion. Let us start with the "screening" term. This term is proportional to the squared FS average of the product of the Raman vertex γ and the Tsuneto function λ . The Tsuneto function in turn is proportional to the square of the gap function. Following Devereaux and Einzel³ we assume a d-wave gap in the form of $\Delta(\vec{k}) = \Delta_{max} \cos 2\phi$, which has a B_{1g} symmetry. When squared it becomes totally symmetric (A_{1g}). Therefore an averaged product of the Raman vertex and Tsuneto function will be nonzero only if the vertex function is totally symmetric. This is not the case for the B_{1g} ($\gamma \sim \cos 2\phi$) and B_{2g} ($\gamma \sim \sin 2\phi$) Raman vertexes, but only for the A_{1g} ($\gamma \sim 1 + \cos 4\phi$) as seen in Fig.1. Therefore A_{1g} scattering component is the only component strongly affected or "screened" by the

long range Coulomb interaction³⁻⁷. Let us now look on the bare Raman response. This term is proportional to the FS average of the product of the squared Raman vertex γ^2 and Tsuneto function λ ($\propto \Delta(\vec{k})^2$). Both γ^2 and λ are totally symmetric. One sees from Fig.1 that maxima and nodes of the squared B_{1g} Raman vertex coincide with that of squared d-wave gap. This leads to the highest relative peak position for the B_{1g} scattering component and a ω^3 -dependence of the low frequency scattering. In contrast, maxima of the B_{2g} Raman vertex coincide with nodes of the squared d-wave order parameter, resulting in a lower relative peak position and a linear-in- ω low frequency dependence for this component. The A_{1g} scattering component is the only one which is screened. The "screening" term shifts the peak position of the A_{1g} scattering component to a frequency smaller than that of the B_{1g} . Because of the "screening" term, one could expect that the A_{1g} ELRS peak should be the weakest one⁵⁻⁷. Nevertheless in all optimally doped HTSC (YBCO⁹⁻¹¹, Bi-2212¹², Tl-2223¹³, La-214¹⁴, Tl-2201^{15,16}) the relative intensity of the A_{1g} ELRS peak is strong and comparable to that of the B_{1g} peak. This contradicts existing LDA-based calculations of the electronic Raman scattering cross-section⁵. However, resonance effects^{18,19} may alter these calculations. This picture qualitatively describes the experimental results for all optimally doped HTSC's. The only exception is the n -type superconductor (Nd,Ce)-214, which demonstrates a behavior consistent with an s-wave type of order parameter²⁰.

For the overdoped or underdoped samples the above mentioned universality of the experimental results does not hold anymore. For instance C. Kendziora et al.²¹ reported for overdoped $Tl_2Ba_2CuO_{6+\delta}$ (Tl-2201) a similar peak position for the different symmetry components of the electronic Raman scattering. The authors pointed out that the gap does not scale with T_c , but rather decreases with an increase of doping, yielding a $2\Delta_0/k_B T_c = 3.9$. This led them to suggest that in the overdoped Tl-2201 the order parameter has s-symmetry. One should note, however, that existing calculations of the ELRS peak positions (especially for the A_{1g} scattering component³⁻⁷) strongly depend on the chosen electronic structure and gap function parameters. For the optimally doped Tl-2201 the difference between the peak positions of the B_{1g} and B_{2g} components is about 10% only¹⁶. One can estimate an expected difference between the corresponding peak positions for strongly overdoped Tl-2201 by scaling the peak position of the B_{1g} scattering component in optimally doped Tl-2201 ($\approx 430 \text{ cm}^{-1}$) to that reported for the strongly overdoped Tl-2201 ($\approx 80\text{-}100 \text{ cm}^{-1}$). Such an estimate gives for the strongly overdoped crystal a peak position of the B_{2g} scattering component at only 8-10 cm^{-1} lower frequency than that of the B_{1g} component. This is actually within experimental error. Therefore the same position of the peaks cannot prove s-wave pairing.

According to Devereaux et al.³, the low frequency power-law behavior of the ELRS intensity is more "robust" concerning changes of the FS topology as a result of overdoping and underdoping. Particularly the ω^3 -law for the low frequency scattering in the B_{1g} scattering component and ω -law for the A_{1g} and B_{2g} scattering components should not change with doping in a d-wave superconductor. Unfortunately the ELRS peaks in strongly overdoped Tl-2201 have their maxima at a rather low frequency, which makes it difficult to determine their low-frequency tails precisely. Additionally the low frequency scattering for the A_{1g} component is easily obscured by Rayleigh scattering. In order to test the low frequency behavior in the overdoped Tl-2201 it is therefore necessary to investigate moderately overdoped samples with a pair-breaking peak not at too low frequency.

In addition to the scattering in the superconducting state the normal state scattering provides important information about carrier dynamics. Raman scattering in the normal state in channel L and assuming a single impurity scattering lifetime τ can be described by a Lorentzian:

$$\Im\chi_L(\omega, T > T_c) = 2N_F\gamma_L^2 \frac{\omega\tau}{(\omega\tau)^2 + 1}, \quad (7)$$

where $\Gamma = 1/\tau$ is the scattering rate, γ_L is a Raman vertex, and N_F is the carrier density of states at the Fermi level^{22,23}. Generally speaking, τ is a function of the scattering channel L and momentum \vec{k} ²⁴. $\Im\chi_L(\omega, T > T_c)$ has a peak at the frequency $\omega = 1/\tau$, and the spectrum falls off as $1/\omega$. Using this fact one can analyze Raman spectra in the normal state and determine how scattering rates change with doping. Hackl et al.²⁵ fitted their data for Bi-2212 using Eq.7 and a frequency dependence of Γ given by the nested Fermi liquid model²⁶. The scattering rates at $T \approx 100 \text{ K}$ were found to be $\Gamma(B_{1g}) \approx 600 \text{ cm}^{-1}$, $\Gamma(B_{2g}) \approx 170 \text{ cm}^{-1}$ for the nearly optimally doped Bi-2212 and $\Gamma(B_{1g}) \approx 160 \text{ cm}^{-1}$, $\Gamma(B_{2g}) \approx 120 \text{ cm}^{-1}$ for overdoped Bi-2212²⁵.

In this paper we present electronic Raman scattering experiments on moderately overdoped $Tl_2Ba_2CuO_{6+\delta}$ with $T_c = 56 \text{ K}$. These are compared with measurements on optimally doped ($T_c = 80 \text{ K}$) and strongly overdoped ($T_c = 30 \text{ K}$) crystals. We show that similarly to optimally doped Tl-2201 also moderately overdoped Tl-2201 samples show a ω^3 -low frequency behavior of the B_{1g} scattering component and a linear low frequency behavior for the B_{2g} scattering component. The above mentioned power laws are consistent with d-wave symmetry of the order parameter. Additionally we will discuss the changes of the relative intensities of the pair breaking peaks in the A_{1g} and B_{1g} scattering components with doping, as well as the electronic Raman scattering in the normal state.

EXPERIMENTAL

We investigated the electronic Raman scattering in the single-CuO₂ layered compound Tl-2201. This provides a single-sheeted Fermi surface²⁷. Therefore the inter-valley scattering due to the multi-sheeted Fermi surface⁵ invoked for the explanation of unexpectedly large A_{1g} scattering intensity does not play a role. Our samples had a shape of rectangular platelets with the size of 2x2x0.15mm. Moderately overdoped and strongly overdoped crystals of Tl-2201 were characterized by a SQUID magnetometer, T_c was found equal to 56±2 K (moderately overdoped) and 30±2 K (strongly overdoped), respectively. The orientation of the crystals was controlled by X-ray diffraction. The Raman measurements were performed in quasi-backscattering geometry. Raman scattering was excited using an Ar⁺-ion laser. The laser beam with 3mW power was focused into a spot of 50μm diameter. The laser induced heating was estimated by increasing the laser power level at a fixed temperature (5 K) and comparing the dependence of the ELRS B_{1g}-peak intensity on laser power with the temperature dependence of the intensity of this peak measured at fixed laser power (3mW). Estimated additional heating was found to be about 12.5±2.5 K (all data are plotted with respect to the estimated temperature). In order to analyze pure scattering geometries we extracted the A_{1g} scattering component from the X'X' (A_{1g}+B_{2g}) and XY (B_{2g}) scattering geometries. The X' and Y' axes are rotated by 45° with respect to the X and Y-axes. The X- and Y-axes are parallel to the Cu-O bonds in the CuO₂ plane of the Tl-2201 unit cell. After subtraction of the dark counts of the detector the spectra were corrected for the Bose-factor in order to obtain the imaginary part of the Raman response function. In order to analyze the low frequency behavior of the B_{1g} scattering component in moderately overdoped Tl-2201 with T_c=56 K we performed measurement in superfluid He (T=1.8 K). This gives us several advantages: Because of the huge thermal conductivity of superfluid helium we do not have any overheating of the sample due to laser radiation. The absence of overheating allows us to precisely determine the real temperature of the excited volume. For T=1.8 K the Bose factor is equal to zero down to at least 10 cm⁻¹. Therefore down to 10 cm⁻¹ we actually measure the imaginary part of the Raman response function.

RESULTS AND DISCUSSION

The Raman spectrum of Tl-2201 shows several phonons and a broad electronic continuum. The superconducting transition leads to the redistribution of the continuum into a broad peak. In Figs.2-4 we show the B_{1g}, A_{1g} and B_{2g} scattering components of the Raman scattering for $T \ll T_c$ (solid line) and $T > T_c$ (dashed line) for the Tl-2201 single crystals with T_c =80 K (Fig.2), T_c =56 K (Fig.3), and T_c =30 K (Fig.4). In order to emphasize the redistribution of the scattering intensity in the superconducting state compared to the normal state we draw not only the Bose-factor-corrected raw spectra (Figs.2, 3 and 4, upper panel), but we subtract the spectra above T_c from the spectra well below T_c (Fig.2, 3 and 4, lower panel). The positions of the ELRS peaks in the superconducting state for different scattering components as a function of doping are summarized in Table I.

It is generally accepted that the B_{1g} scattering component reflects much of the properties of the superconducting density of states⁶. Therefore it is reasonable to analyze intensities of other components relative to the B_{1g} scattering component.

There are several differences between optimally- and overdoped crystals.

i) If one identifies the peak in the B_{1g} ELRS component as a $2\Delta_0$ one obtains the reduced gap value $2\Delta_0/k_B T_c \approx 7.8$ for the optimally doped crystal, while in the overdoped crystals $2\Delta_0/k_B T_c$ is close to 3, (see Table I).

ii) For the optimally doped crystals the peak positions of the B_{2g} and A_{1g} scattering components are lower than that of the B_{1g}, (see Fig.2 and Table I). In the overdoped crystals the B_{2g} component peaks at a frequency very close to that of the B_{1g} scattering component (see Figs.3, 4 and Table.I.), although its peak position is still about 10±2% lower (similar to the optimally doped Tl-2201, see Table I). The A_{1g} peak position is close to that of the B_{1g} peak as well, although an exact determination of the pair-breaking peak position for the A_{1g} scattering component is difficult due to the A_{1g} phonon at 127 cm⁻¹ of moderately overdoped Tl-2201, (see Fig.3) or due to the superimposed Rayleigh scattering in strongly overdoped Tl-2201 (see Fig.4).

iii) The most drastic changes of the relative ELRS peak intensity with doping are seen in the A_{1g} scattering component. For the optimally doped crystal we observe a strong peak, which is comparable in intensity to that of the B_{1g} component, see Fig.2a and b, lower panel. In contrast, for two overdoped crystals (Figs.3, 4 a and b, lower panel) the relative intensity of the ELRS peak in the A_{1g} scattering component is weak.

iiii) In contrast to the A_{1g} scattering component the intensity of the B_{1g} scattering component is stronger in the moderately overdoped sample (Fig. 3a) compared to the optimally doped one (Fig. 2a). For the strongly overdoped sample an exact determination of the relative intensity of the pair-breaking peak is difficult in all scattering components. The pair-breaking peak is at too low frequency (≈ 60 cm⁻¹), therefore its intensity is very sensitive to the Bose-factor correction, which in turn depends upon the uncertainty in the estimated temperature. Additionally,

Rayleigh scattering and impurity induced scattering³ may obscure the evaluated difference between the corresponding spectra below and above T_c .

According to Devereaux et al.³, the ω^3 -law for the low frequency scattering in the B_{1g} scattering component and the ω -law for the A_{1g} and B_{2g} scattering components should not change with doping in d-wave superconductors. In order to check these power laws for the moderately overdoped Tl-2201 we have performed measurements in superfluid helium ($T=1.8$ K). To illustrate the low frequency behavior of the imaginary part of the Raman response function in the B_{1g} and B_{2g} scattering components on the same frequency scale we have scaled the Raman shift by the corresponding peak position, as shown in Fig. 5a. The fit of the low frequency scattering in the B_{1g} scattering component with the ω^n -function leads to exponents $n=2.9$ and 3.5 for the optimum doped and moderately overdoped Tl-2201, respectively. An even better fit to the low frequency scattering intensity in moderately overdoped Tl-2201 was obtained with a linear term added to the ω^n function, similarly to overdoped Bi-2212²⁵. The appearance of such a crossover from linear to a power law in the B_{1g} scattering component indicates the presence of impurities³. For the B_{2g} scattering component one can easily fit the low frequency scattering of optimally to overdoped samples with a linear-in- ω law as shown in Fig.5b. Unfortunately in the $T_c=30$ -K crystal the expected ELRS peak is too close to zero frequency to make a definite conclusion about its low frequency behavior. The observed power laws (Fig.5) lead to the conclusion that even overdoped Tl-2201 has a d-wave symmetry of the order parameter.

Let us now discuss temperature induced spectral changes in the overdoped crystal. A detailed temperature dependence for the Tl-2201 ($T_c=56$ K) sample is shown for the B_{1g} component in Fig.6. With increasing temperature the intensity of the pair-breaking peak decreases and its position shifts toward lower frequency. This dependence slightly differs from that predicted by the BCS theory, as shown in the inset of Fig.6, i.e. the gap opens more abruptly. At the same time the intensity of the pair-breaking peak decreases nearly linearly with increasing temperature (see insert in Fig.7) whereas the intensity of the low frequency scattering (at for instance ≈ 50 cm^{-1}) increases. At a temperature close to T_c both intensities match. From this data one can determine the ratio of the superconducting response to the normal state response in the static limit ("static ratio"), i.e. when $\omega \rightarrow 0$ and compare it with the calculations of the ratio in the presence of impurities⁴. From such a comparison we found for the moderately overdoped Tl-2201 the corresponding value of the scattering rate to be $\Gamma/\Delta(0) \approx 0.5$. This leads to $\Gamma \approx 60$ cm^{-1} . In the normal state spectra (we discuss the imaginary part of the Raman response function) one sees an increase of the intensity towards zero with a broad peak at ≈ 50 cm^{-1} , Figs.3 and 7. This peak is more pronounced in the B_{1g} scattering component. Such a peak can be attributed to impurity induced scattering. According to Eq.7 the frequency of the peak corresponds to the scattering rate $\Gamma = 1/\tau$ of the normal state^{22,23}. The position of the peak depends strongly on doping. It is roughly 35 or 50 cm^{-1} for strongly and moderately overdoped Tl-2201, respectively. Practically there is no anisotropy of the peak position comparing the B_{1g} and B_{2g} scattering components. Note that the scattering rates calculated from the peak positions are very close to that evaluated from the "static ratio" and sufficiently smaller than that found by Hackl et al.²⁵ using a frequency dependence of Γ given by the nested Fermi liquid model. Scattering rates may also be determined using the frequency dependent conductivity from the infrared measurements. One finds for many HTSC scattering rates $1/\tau$ of about 100-200 cm^{-1} at $T \approx 100$ K²⁸. Additionally and very surprisingly, the scattering rates decrease with increasing overdoping²⁹. From our Raman measurements we found scattering rates $\Gamma = 1/\tau = 35$ or 50 cm^{-1} for strongly and moderately overdoped Tl-2201 not too far from the infrared data, and a similar decrease of Γ with increasing overdoping.

We would like to sum up the effects of overdoping that are also partly observed in other HTSC:

In the nearly optimally doped regime (YBCO⁹⁻¹¹, Bi-2212¹², Tl-2223¹³, La-214¹⁴, Tl-2201^{15,16}) the ELRS peak positions scale with T_c for all scattering components. The B_{1g} scattering component is most sensitive to changes of T_c . The relative intensity of the ELRS A_{1g} peak is stronger or at least comparable to that of the B_{1g} component. The relative intensity of the B_{2g} peak is always the weakest one.

For the overdoped crystals (Tl-2201, Bi-2212)^{21,25} the peak position of the B_{1g} scattering component decreases faster than T_c so that $2\Delta_0/k_B T_c$ decreases with overdoping from 7.4 to ≈ 3 (data of this paper), or from 8 to 5 in Bi-2212²⁵. The relative intensity of the A_{1g} ELRS peak as compared to B_{1g} decreases when the system becomes more overdoped³⁰. This is an important point concerning the influence of the Fermi surface topology changes on Raman scattering and will be discussed further below.

We will now discuss some reasons which may explain the shift of the B_{1g} peak position with doping. The decrease of the B_{1g} ELRS peak position and $2\Delta_0/k_B T_c$ with doping is connected to the fact that the crossing of the Fermi surface with the Brillouin zone moves away from the $(0, \pm\pi)$, $(\pm\pi, 0)$ points with doping. Therefore the FS average $\langle \gamma_{\vec{k}}^2 \lambda_{\vec{k}} \rangle$ of the Raman vertex with the Tsuneto function in Eq.2 gives a Δ_0 smaller than Δ_{max} . A detailed discussion of this point is given in the work of Branch and Carbotte⁶. In the case of optimum doping it is supposed that the Fermi level is close to the van Hove singularity (vHs) so that the FS pinches at the $(0, \pm\pi)$, $(\pm\pi, 0)$ points of the BZ³¹ leading to $\Delta_0 \approx \Delta_{max}$.

Now let us turn to the decrease of the A_{1g} vs. B_{1g} intensities of the ELRS with doping. In contrast to B_{1g} and

B_{2g} the A_{1g} scattering component is affected by the screening term. We suppose that "screening" itself is connected with the FS anisotropy, which is in turn affected by the van Hove singularity. In optimally doped crystals vHs is close to the Fermi level (FL) leading to strongly anisotropic FS. By overdoping we move FL from vHs. This leads to a more isotropic FS with larger "screening". Therefore the increase of "screening" with doping would be a plausible explanation for the observed decrease of the A_{1g} scattering component with doping.

This suggestion has a consequence for the intensity of the B_{1g} scattering component. Namely the "screening" term for the A_{1g} scattering component has the same symmetry as the bare term for the B_{1g} scattering component (see Fig.1). If we suppose that the "screening" increases, the B_{1g} response should also increase. This is in agreement with our results (see Figs. 2a and 3a, lower panel).

In conclusion we have presented measurements of the electronic Raman scattering on optimally doped as well as moderately and strongly overdoped Tl-2201 single crystals. The strong decrease of the A_{1g} scattering intensity with increasing overdoping has been observed. We connect this effect with the changes of the FS topology connected to the existence of a van Hove singularity. We propose investigations on other overdoped HTSC in order to check this idea. Our measurements of the low frequency behavior of the electronic Raman scattering in optimally doped and moderately overdoped Tl-2201 confirmed a d-wave symmetry of the order parameter, in contrast to earlier reports²¹. The scattering rates, we have evaluated from the normal state Raman spectra as well as a decrease of them with overdoping are consistent with the existing infrared data.

ACKNOWLEDGMENTS

This work was supported by DFG through SFB 341, BMBF FKZ 13N7329 and INTAS grants 94-3562 and 96-410. One of us (L.V.G.) acknowledges support from the Alexander von Humboldt Foundation.

-
- ¹ A.A. Abrikosov and V.M. Genkin, Sov. Phys.-JETP 38, 417 (1973).
² M.V. Klein and S.B. Dierker, Phys. Rev. B 29, 4976 (1984).
³ T.P. Devereaux, D. Einzel, Phys. Rev. B 51, 16336 (1995).
⁴ T.P. Devereaux and A. Kampf, unpublished.
⁵ T. Strohm, and M. Cardona, Phys. Rev. B 55, 12725 (1997).
⁶ D. Branch and J.P. Carbotte, Phys. Rev. B 54, 13288 (1996).
⁷ F. Wenger and M. Käll, Phys. Rev. B 55, 97 (1997).
⁸ X.K. Chen, J.G. Naeini, K.C. Hewitt and J.C. Irwin, R. Liang, W.N. Hardy, (unpublished).
⁹ R. Hackl, W. Glaser, P. Müller, D. Einzel, and K. Andres, Phys. Rev. B 38, 7133 (1988).
¹⁰ S.L. Cooper, F. Slakey, M.V. Klein, J.P. Rice, E.D. Bukowski, and D.M. Ginsberg, Phys. Rev. B 38, 11934 (1988).
¹¹ X.K. Chen, E. Altendorf, J.C. Irwin, R. Liang, and W.N. Hardy, Phys. Rev. B 48, 10530 (1993).
¹² T. Stauffer, R. Nemetschek, R. Hackl, P. Müller, and H. Veith, Phys. Rev. Lett. 68, 1069 (1992).
¹³ A. Hoffmann, P. Lemmens, G. Güntherodt, V. Thomas, and K. Winzer, Physica C 235-240, 1897 (1994).
¹⁴ X.K. Chen, J.C. Irwin, H.J. Trodahl, T. Kimura, and K. Kishio, Phys. Rev. Lett. 73, 3290 (1994).
¹⁵ R. Nemetschek, O.V. Misochko, B. Stadlober, and R. Hackl, Phys. Rev. B 47, 3450 (1993).
¹⁶ L.V. Gasparov, P. Lemmens, M. Brinkman, N.N. Kolesnikov, G. Güntherodt, Phys. Rev. B 55, 1223 (1997).
¹⁷ T. Tsuneto, Phys. Rev. 118, 1029 (1960).
¹⁸ M. Kang, G. Blumberg, M.V. Klein and N.N. Kolesnikov, Phys. Rev. Lett. 77, 4434 (1996).
¹⁹ E. Ya. Sherman, (unpublished). It has been shown here that anisotropy of the Raman vertex does not follow the effective mass anisotropy even away from a resonance.
²⁰ B. Stadlober, G. Krug, R. Nemetschek, and R. Hackl, Phys. Rev. Lett. 74, 4911 (1995).
²¹ C. Kendziora, R. Kelley and M. Onellion, Phys. Rev. Lett. 77, 727 (1996).
²² A. Zawadowski and M. Cardona, Phys. Rev. B 42, 10732 (1990).
²³ V.N. Kostur, Z. Phys. B 89, 149 (1992).
²⁴ O.V. Misochko, E. Ya. Sherman., Int. J. Mod. Phys. B 24, 3371 (1994).
²⁵ R. Hackl, M. Opel, P. Müller, G. Krug, B. Stadlober, R. Nemetschek, H. Berger, L. Forro, Journal of Low Temp. Phys. 105, 733 (1996).
²⁶ A. Virosztek et al., Phys. Rev. B 45, 347 (1992).
²⁷ V.V. Tatarskii, M. Paranthaman, and A.M. Hermann, Phys. Rev. B 47, 14489 (1993).

- ²⁸ D.B. Tanner and T. Timusk, Optical properties of High- Temperature Superconductors in Physical Properties of High Temperature superconductors III, edited by D.M. Ginsberg, World Scientific, Singapore, New Jersey, London, Hong Kong, 1992.
- ²⁹ A.V. Puchkov, P. Fournier, T. Timusk, and N.N. Kolesnikov Phys. Rev. Lett. 77, 1853 (1996).
- ³⁰ G. Blumberg, private communication.
- ³¹ D.L. Novikov and A.J. Freeman, Recent Developments in High Temperature Superconductivity, eds. J. Klamut et al., Springer series Lecture notes in Physics, V.475, 17 (1995).

FIG. 1. Schematic representation of the Raman response function in Eq.2 due to the breaking of Cooper pairs and including Coulomb repulsion. The Tsuneto function $\lambda_{\vec{k}}$ is represented as a squared gap function $\Delta^2(\vec{k}) = \Delta_{max}^2 \cos^2 2\phi$. Raman vertices are chosen as $\gamma_{B_{1g}} \propto \cos 2\phi$, $\gamma_{B_{2g}} \propto \sin 2\phi$, $\gamma_{A_{1g}} \propto 1 + \cos 4\phi$, where ϕ is an angle between \vec{k} and the Cu-O bond direction within the CuO₂ plane.

FIG. 2. Imaginary part of the Raman response in optimally doped Tl-2201 ($T_c=80\pm 5$ K) at T=20 K (solid curve), and T=110 K (dashed curve) for the a) B_{1g} , b) A_{1g} , and c) B_{2g} scattering components (upper panel) and for the corresponding subtracted spectra: $\Im\chi(T=20\text{ K}) - \Im\chi(T=110\text{ K})$ (lower panel).

FIG. 3. Imaginary part of the Raman response in moderately overdoped Tl-2201 ($T_c=56\pm 2$ K) at T=20 K (solid curve), and T=75 K (dashed curve) for the a) B_{1g} , b) A_{1g} , and c) B_{2g} scattering components (upper panel) and for the corresponding subtracted spectra: $\Im\chi(T=20\text{ K}) - \Im\chi(T=75\text{ K})$ (lower panel).

FIG. 4. Imaginary part of the Raman response in strongly overdoped Tl-2201 ($T_c=30\pm 2$ K) at T=15 K (solid curve), and T=50 K (dashed curve) for the a) B_{1g} , b) A_{1g} , and c) B_{2g} scattering components (upper panel), and for the corresponding subtracted spectra: $\Im\chi(T=15\text{ K}) - \Im\chi(T=50\text{ K})$ (lower panel).

FIG. 5. Imaginary part of the Raman response in optimally doped ($T_c=80\pm 5$ K, dashed line, at T=20 K), moderately overdoped ($T_c=56\pm 2$ K, dash-dotted line, at T=1.8 K), and strongly overdoped ($T_c=30\pm 5$ K, dotted line, at T=15 K) Tl-2201 for the a) B_{1g} and b) B_{2g} scattering components. For each doping and scattering component the frequency-axis is rescaled to the position of the respective pair-breaking peak. The solid curves show fits to the low frequency scattering with the a) $\Im\chi \sim \omega^n$ ($n=2.9$ and 3.5 for the crystals with $T_c=80\pm 5$ K and 56 ± 2 K, respectively) and b) $\Im\chi \sim \omega$ function.

FIG. 6. Temperature dependence of the Raman scattering intensity of the B_{1g} scattering component in the moderately overdoped Tl-2201 ($T_c=56\pm 2$ K) without corrections of the Bose-factor. With increase of the temperature the pair-breaking peak position of the ELRS shifts to lower frequency and its intensity decreases. The insert shows the temperature dependence of the pair-breaking peak position (solid circles) and the expected dependence from BCS theory (solid line). Note that at $T=59\text{ K} > T_c = 56\text{ K}$ one sees a characteristic increase of the intensity towards zero frequency which is attributed to impurity induced scattering.

FIG. 7. Imaginary part of the Raman response function at $T \leq T_c$, with T=55 K (solid line), T=48 K (dashed line) and T=45 K (dotted line) for the B_{1g} scattering component of moderately overdoped Tl-2201. Arrows show the pair-breaking peak ($\approx 105\text{ cm}^{-1}$ at T=45 K) and the peak due to scattering on the "normal excitations" ($\approx 50\text{ cm}^{-1}$). The insert shows a temperature dependence of the pair-breaking peak intensity (solid squares) and the intensity of the "normal excitation" scattering (open squares) in the B_{1g} scattering component in the moderately overdoped Tl-2201 ($T_c=56\pm 2$ K).

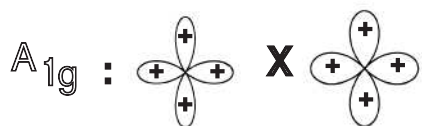
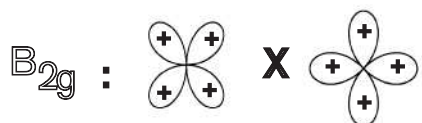
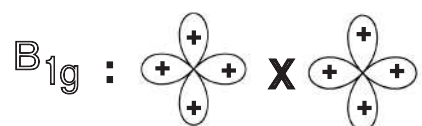
TABLE I. Peak positions of the B_{1g} , A_{1g} and B_{2g} electronic Raman scattering components, for optimally and overdoped Tl-2201.

Compound Tl-2201	T_c [K]	B_{1g} [cm^{-1}]	A_{1g} [cm^{-1}]	B_{2g} [cm^{-1}]	$2\Delta_{max}/k_B T_c$
optimally doped	80 ± 5	430 ± 15	345 ± 20	380 ± 35	7.8 ± 0.4
moderately overdoped	56 ± 2	125 ± 10	110 ± 20	120 ± 10	3.3 ± 0.3
strongly overdoped	30 ± 2	60 ± 5	?	50 ± 5	2.9 ± 0.4

Question mark (?) indicates no detection of a pair-breaking peak.

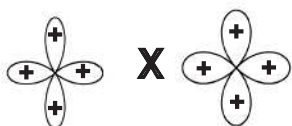
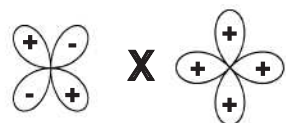
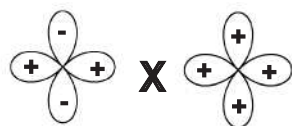
Bare

$$\gamma^2 \times \lambda (\Delta^2)$$



Screening

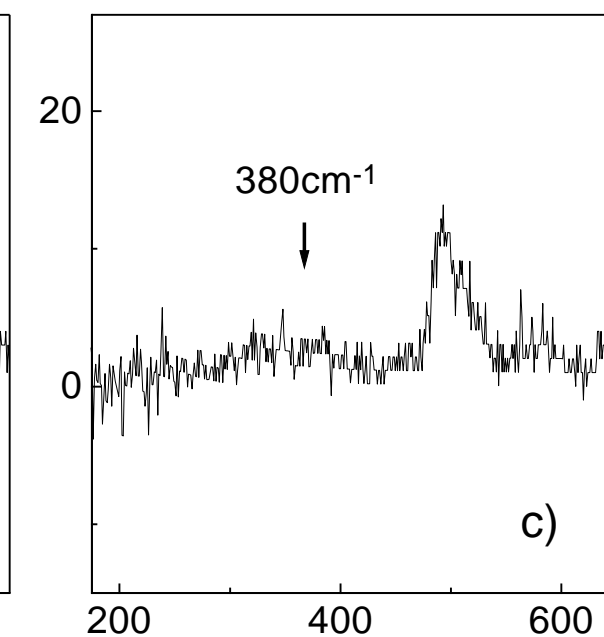
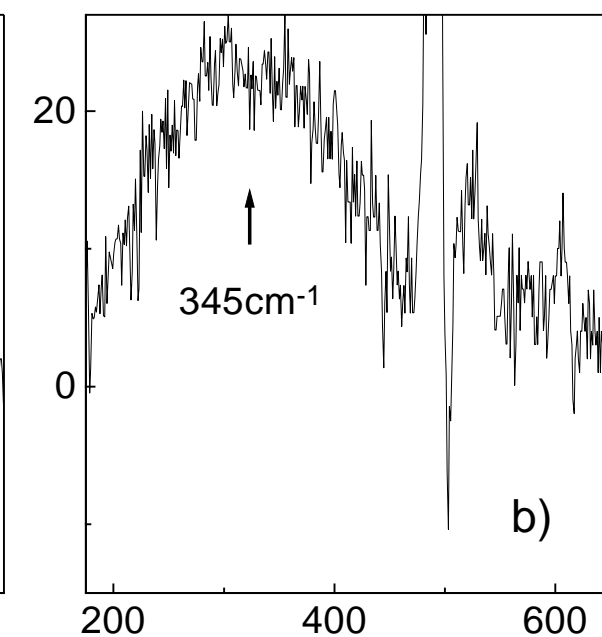
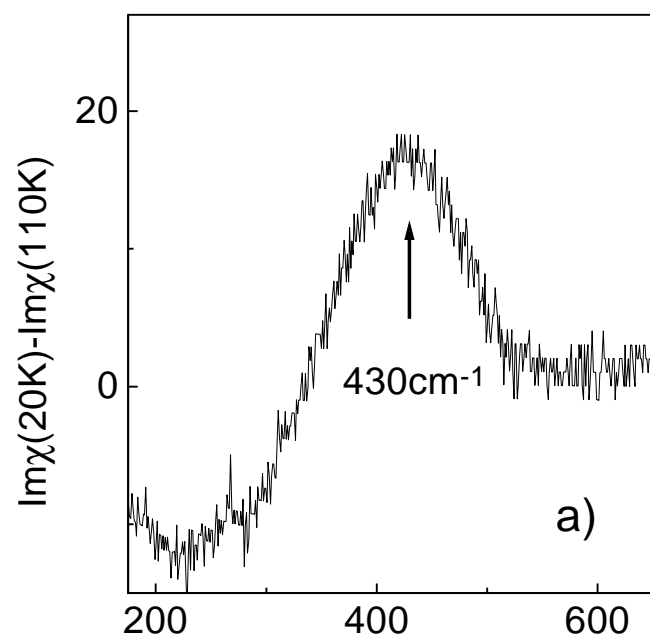
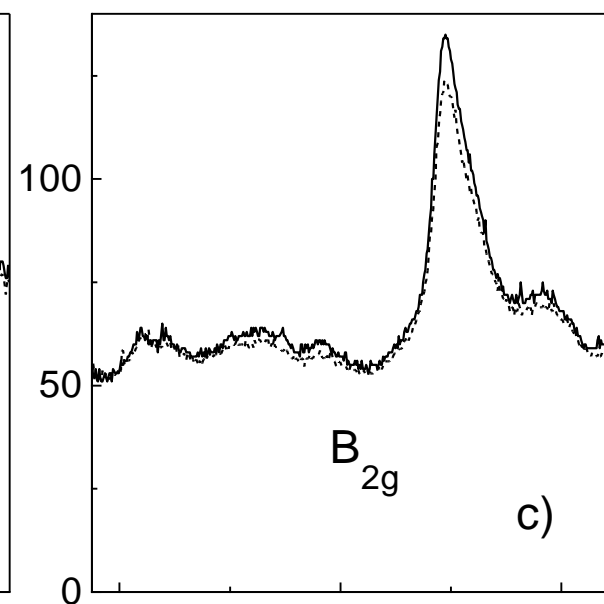
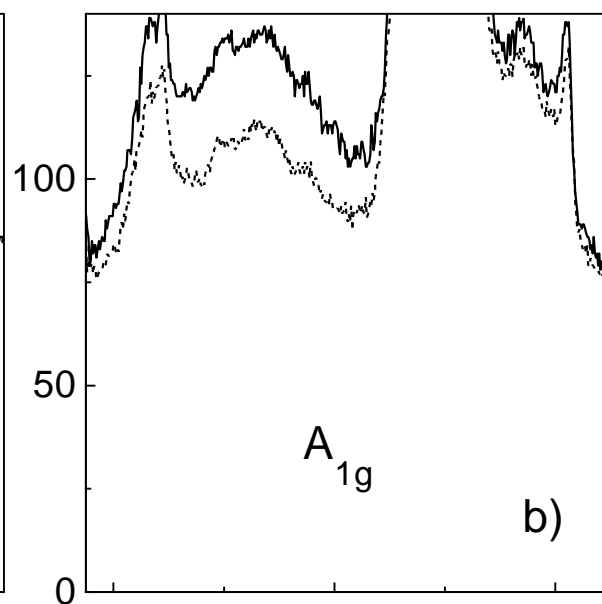
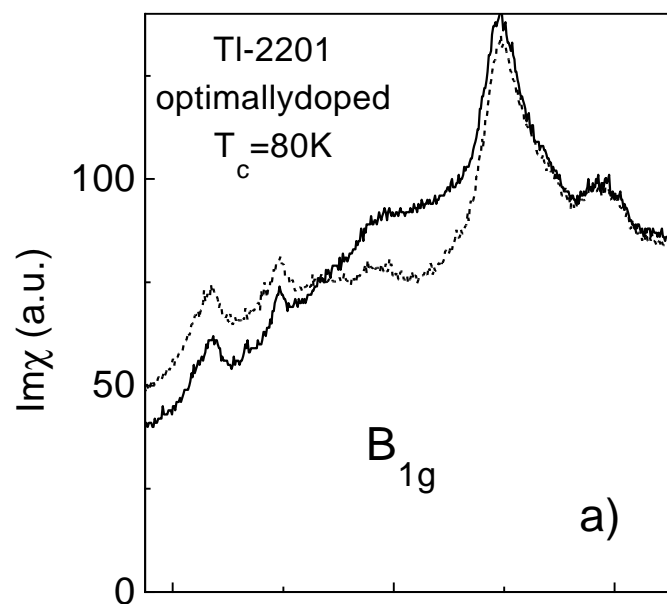
$$\gamma \times \lambda (\Delta^2)$$



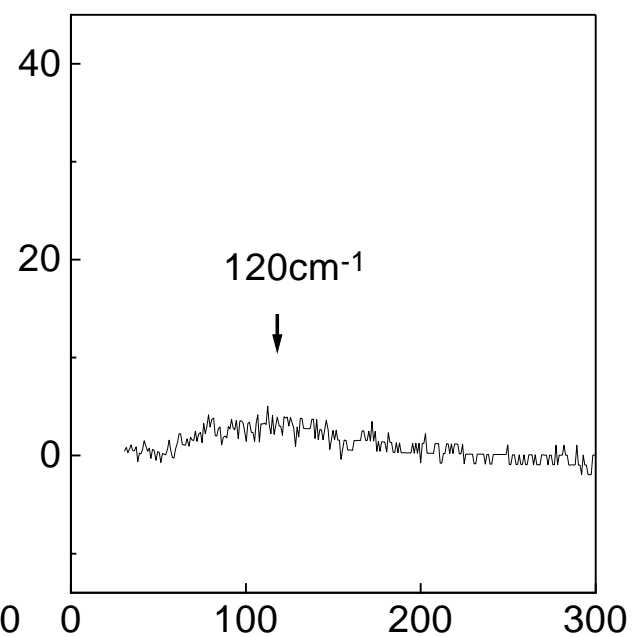
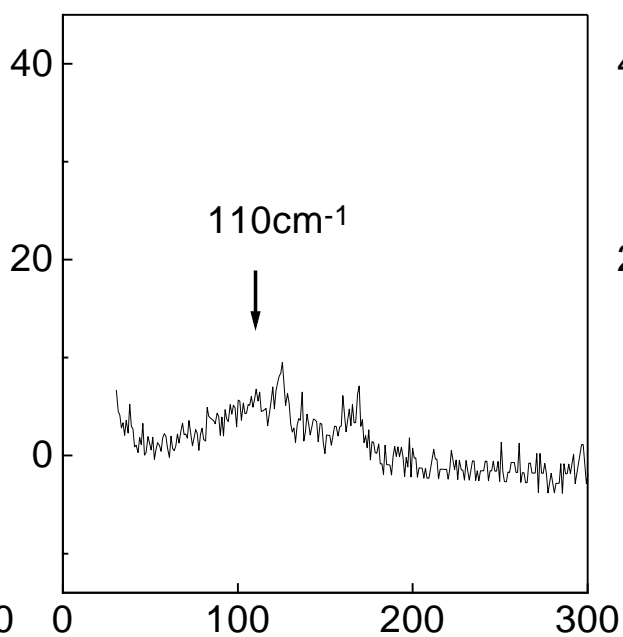
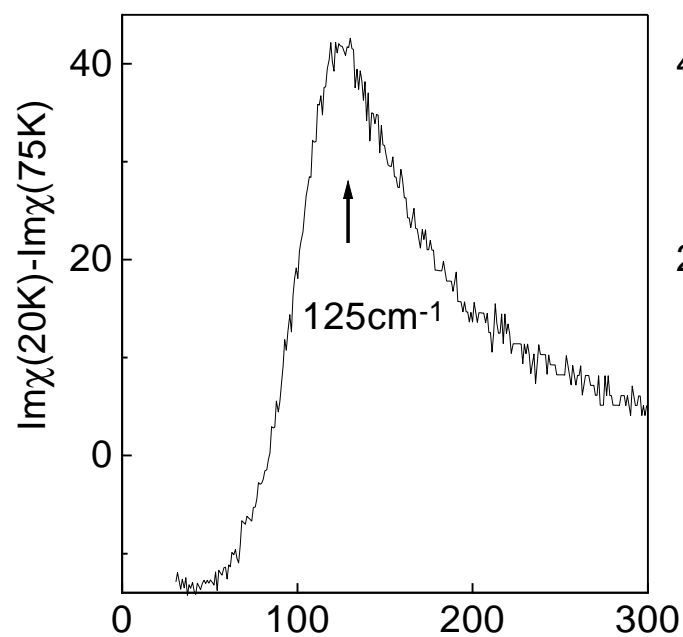
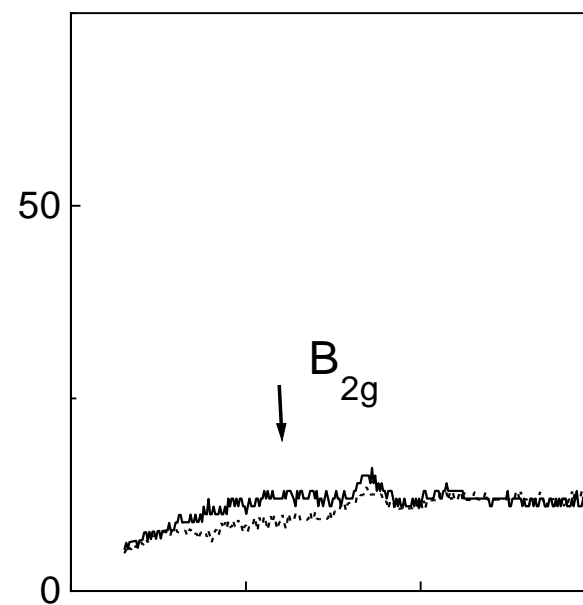
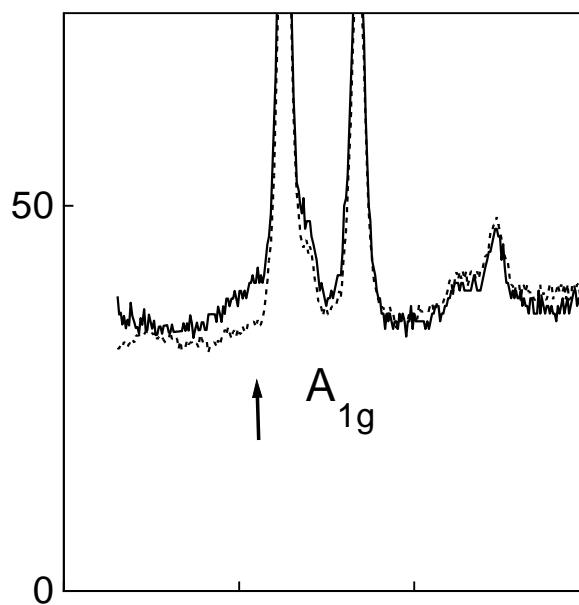
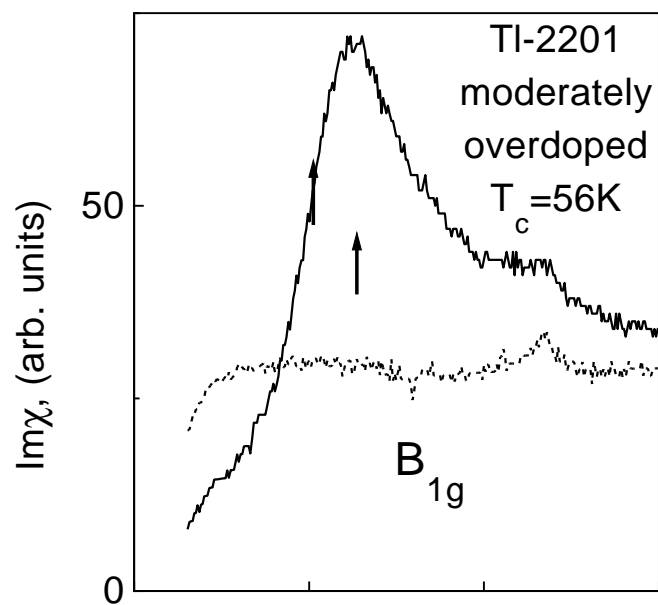
—

—

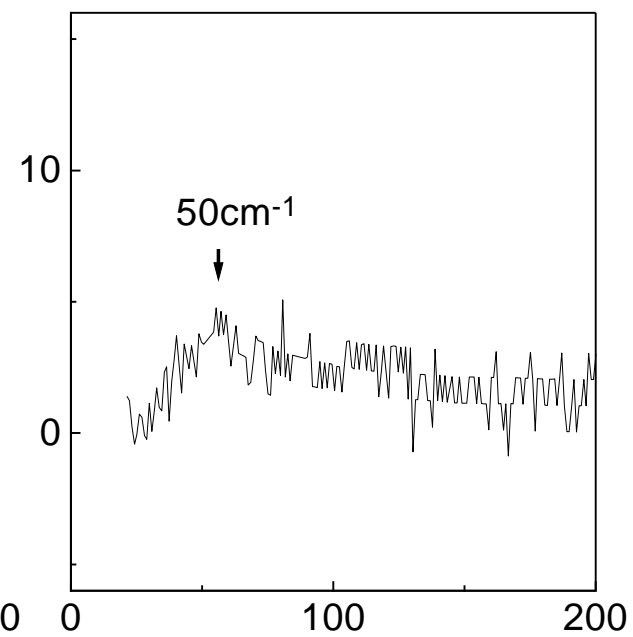
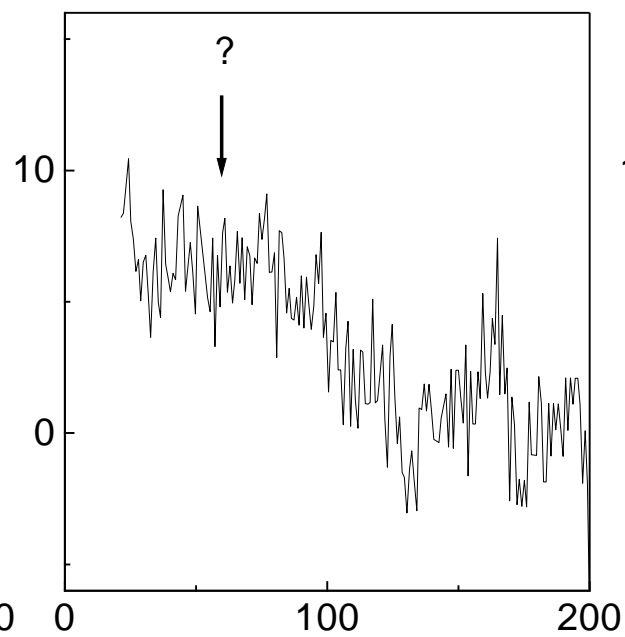
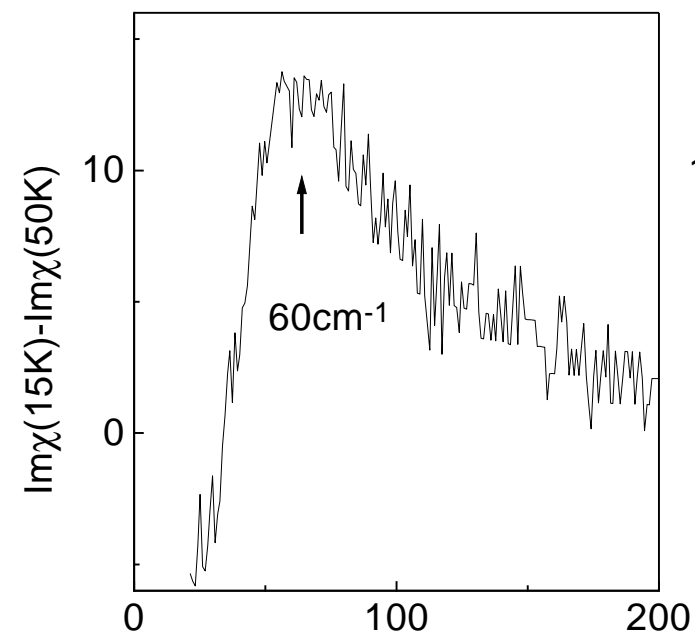
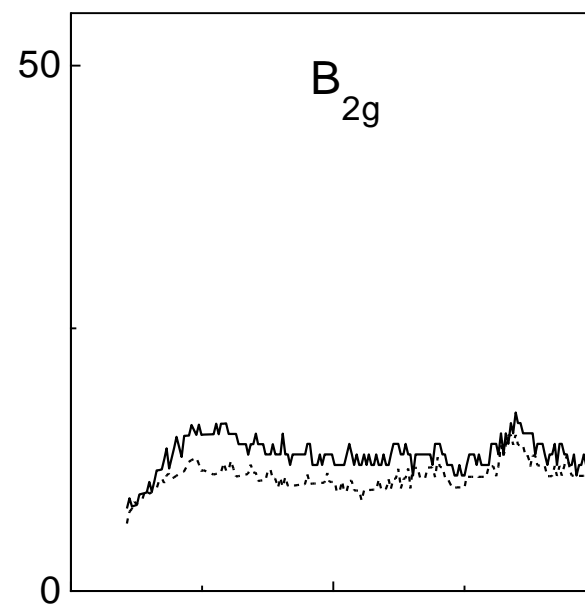
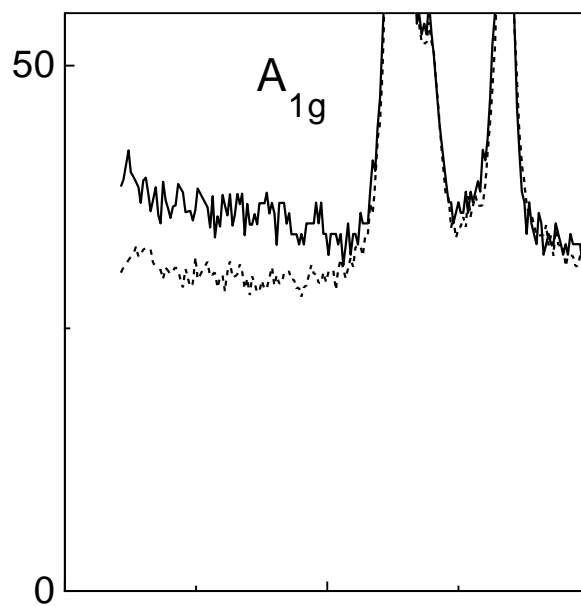
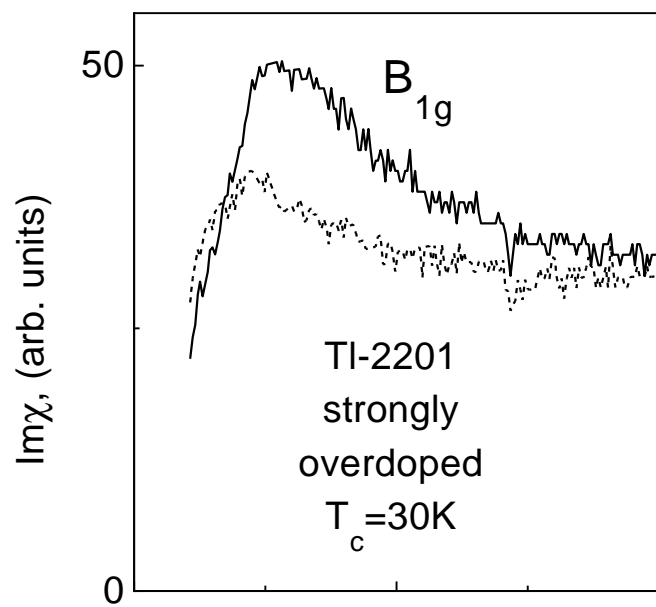
—



Wave numbers (cm^{-1})



Wave numbers, cm^{-1}



Wave numbers, cm^{-1}

